Active Flow Control Systems Architectures for Civil Transport Aircraft

M. Jabbal,* S. C. Liddle,† and W. J. Crowther‡
University of Manchester, Manchester, England M60 1QD, United Kingdom

DOI: 10.2514/1.C000237

This paper considers the effect of choice of actuator technology and associated power systems architecture on the mass cost and power consumption of implementing active flow control systems on civil transport aircraft. The research method is based on the use of a mass model that includes a mass due to systems hardware and a mass due to the system energy usage. An Airbus A320 aircraft wing is used as a case-study application. The mass model parameters are based on first-principle physical analysis of electric and pneumatic power systems combined with empirical data on system hardware from existing equipment suppliers. Flow control methods include direct fluidic, electromechanical-fluidic, and electrofluidic actuator technologies. The mass cost of electrical power distribution is shown to be considerably less than that for pneumatic systems; however, this advantage is reduced by the requirement for relatively heavy electrical power management and conversion systems. A tradeoff exists between system power efficiency and the system hardware mass required to achieve this efficiency. For short-duration operation the flow control solution is driven toward lighter but less power-efficient systems, whereas for long-duration operation there is benefit in considering heavier but more efficient systems. It is estimated that a practical electromechanical-fluidic system for flow separation control may have a mass up to 40% of the slat mass for a leading-edge application and 5% of flap mass for a trailing-edge application.

Nomenclature

A = cross-sectional area of pipe, orifice, or exposed plasma electrode, m^2
a = actuator diaphragm peak-to-peak displacement, m
D = drag offtake associated with a flow control system, N
D_i = internal diameter of pipe; diameter of wire, m
d = orifice diameter, m
E = fuel usage, gal
F = output force of active surface membrane actuator, N
f = friction factor; frequency, Hz
H = number of airborne hours
I = current, A
L = distribution length of pipe or wire, m
M = Mach number
m = overall mass of flow control system, kg
$\dot{m}$ = mass flow rate, kg/s
m_d = distribution mass, kg
m_{fuel} = fuel mass required for flow control operation, kg
m_w = power-specific mass of a system component, kg/kW
m'_{wd} = power distribution specific mass per unit length, kg/kWm
$\dot{m}_{Wg}$ = power generation specific fuel mass flow rate, kg/kWs
n = number of actuators
P = pressure, Pa
R = wire resistance, ohms; universal gas constant, m^{3}Pa/Kmol
  =
Re = pipe Reynolds number

S = number of aircraft seats
s_A = spanwise extent of actuator array, m
T = temperature, K; period of oscillation, s
U = pipe flow velocity, m/s
U_j = actuator jet velocity, m/s
U_∞ = freestream velocity, m/s
V = average aircraft speed, mph; voltage, V
V_R = actuator jet to freestream velocity ratio
W_E = electrical power, W
W_F = flow (fluid) power, W
W_P = pressure power, W
Δ = ratio of orifice diameter to local boundary-layer height
ΔP = pressure drop, Pa
ΔV = voltage drop, V
Δt = operation duration of flow control system, s
δ = boundary-layer height, m
η = overall power efficiency of flow control system
η_d = power distribution efficiency
λ = ratio of actuator spanwise spacing to orifice diameter
ρ = fluid density, kg/m^3
τ = pulse duty cycle

I. Introduction

W HILE there has been some progress toward identifying suitable fluidic actuator concepts for application on commercial transport aircraft, there is still considerable uncertainty as to the nature of the systems architectures that are needed to support the generation, management, and distribution of power to these actuators. In particular, the choice between distributing power electrically or pneumatically is still an open question, despite significant historical development of boundary-layer control technologies using compressed air [1] and progress toward the development of the more electric aircraft [2].

For pneumatic flow control technologies, compressed air is needed at the point of delivery at the actuator; hence, direct bleed of compressed air from an engine initially appears to provide a very competitive power option. However, there are issues in that the amount of bleed air available is correlated with the engine throttle setting, which may severely limit bleed availability at low-throttle conditions: e.g., landing. Furthermore, the pipework required for ducting compressed air is relatively heavy, compared to a system for

*Research Associate, School of Mechanical, Aerospace and Civil Engineering, P.O. Box 88, Sackville Street; mark_jabbal@hotmail.com.
†Research Associate, School of Mechanical, Aerospace and Civil Engineering, P.O. Box 88, Sackville Street.
‡Senior Lecturer, School of Mechanical, Aerospace and Civil Engineering, P.O. Box 88, Sackville Street.

Table 1   Power systems breakdown by application for a conventional civil transport aircraft[a]

	Electric	Hydraulic	Pneumatic
Primary Source	Engine-driven generators	Engine-driven pumps	Engine bleed
Secondary/emergency sources	APU/RAT/batteries	APU/RAT	APU
Transmission system	Cabling from electric power buses	Ducting	Ducting from bleed manifold
Applications	Galley systems, cabin/IFE systems, lighting, and avionics	Control surface actuation, undercarriage actuation, and high-lift system actuation	Cabin pressurization, anti-icing, and engine starting (from ground or APU supply)
Notable certification requirements	Source redundancy from multiple main generators and (particularly for ETOPS) APU and bus (distribution) redundancy	Multiple redundant transmission systems and pressurization in event of primary failure by RAT	Limited maximum temperature to avoid autoignition of leaking fuel and cross-feed supply to allow for engine failure

[a]RAT denotes ram air turbine, IFE denotes in-flight entertainment, and ETOPS denotes extended-range twin-engine operational performance standards.

delivering the same amount of power electrically, and there are significant maintenance costs associated with pressurized systems with many joints.

For electric solutions, an engine-mounted generator is used to generate electrical power, which is then distributed using wires. However, electrical power has to be converted back into the fluidic domain at the actuator through some form of electromechanical-fluidic transduction. The additional conversion steps involved in electrical power generation and distribution for fluidic flow control actuators means that it takes considerable engineering effort to design electrical generation/distribution/conversion systems that match the mass efficiency of pneumatic-only systems. That said, mass reduction and efficiency of electrical machines and digital power systems continues to improve, while there seems to be little scope for similar improvement in pneumatic systems. Therefore, it is likely that the balance will shift further toward electric power generation and distribution for flow control systems in the future.

Traditionally civil transport aircraft have used hydraulic, electric, and pneumatic systems to transmit power around the aircraft, with different choices for different service applications. However, in more recent designs, including the production Boeing 787, the large majority of systems are electrically powered. The generation system is therefore of greater power capacity when compared to corresponding previous practice. For example, the engine-driven generators of the 787 are of 1000 kVA capacity, compared to the conventional power architecture Boeing 767, which has only 180 kVA, but is comparable in terms of mission. Table 1 gives details of typical applications for each of these systems in an aircraft of conventional architecture. In the Boeing 787, which may be considered to be representative of some future designs, all of the applications identified here are electrically powered with the exception of engine intake anti-icing.

The purpose of the present work is specifically to allow meaningful comparisons to be made between different flow control (FC)[§] methods, in terms of mass cost and power consumption, for operation on commercial transport aircraft. Previous work [3] has established the design trades associated with application of a single type of electromechanical flow control actuator in the form of a synthetic jet actuator (SJA). The present study extends this work by considering a range of different FC actuator technologies and power generation and conversion architectures.

The aerodynamic benefits of the different FC methods for specific applications, such as lift enhancement and drag reduction, are not considered in this study. The implementation of technologies that alter the efficiency of lift and drag generation is a highly nonlinear problem. The authors note, as an example, the analysis of Ning and Kroo [4]. Their study compares the effect on drag of implementing

winglets and wingtip extensions on a civil transport aircraft wing, in each case by presenting optimized overall wing designs that take advantage of the revised tip: a nonlinear comparison. Crucially, however, the basic system impact and design requirements are well known and the ability to evaluate the effect on performance is established; there can be a high degree of confidence that wing performance can be calculated. The state of the art of FC systems engineering has not reached this standard. The technology readiness level of the FC actuators considered is currently far below that which would allow successful implementation on a transport aircraft. There is little empirical data or developed theory on the performance of flight-standard FC systems. Recognizing that this will be an issue for the foreseeable future, the present study focuses on providing information on the implementation costs of FC systems, for which there is currently little reliable information. This requires the assumption to be made in advance that these FC systems would be able to provide the required flow control benefit. By choosing appropriate case studies, it is possible to compare the *relative* impacts of different strategies, while noting that the nonlinear *absolute* impact of using any FC system would not be fully captured. The conclusions drawn in terms of trends, however, remain valid.

II.   Flow Control Systems Architectures

A.   Overview

To aid meaningful comparison of different FC systems, it is useful to define the overall systems architectures required to support FC integration into civil transport aircraft. For the present study, the reference aircraft is the Airbus A320 civil transport aircraft. The overall aircraft power systems architecture is a series of interacting systems, comprising power generation systems, power transformation systems, power distribution systems, and power consumption systems [5,6]. These different systems are interconnected via exchanged energy: e.g., fuel, electric, hydraulic, pneumatic, mechanical and thermal energy.

It is proposed to classify FC systems architectures in a similar manner to the aircraft power systems architecture. For the present work, *architecture* is defined as the combination of an actuator technology and the means of delivering power to it. An FC systems architecture specifically consists of generation, management, distribution and actuator systems. Energy exchanges or transductions occur at the start (generation) and end (actuator) of the power distribution system. The actuator type is known a priori, and thus consideration of the different actuator systems will allow for different distribution systems to be defined.
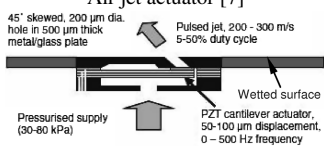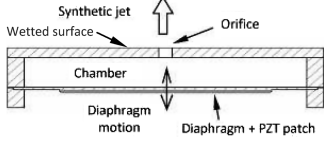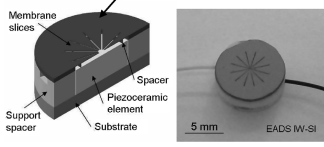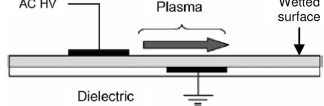
B.   Actuator Systems

Table 2 provides a summary of the main FC actuators considered. The actuators are defined in terms of three characteristics:

1) Transduction is the process by which the actuator transforms and delivers energy to an external flow.

2) Topology is the shape and orientation of the actuator interface with an external flow.

3) Mechanism is the means by which the actuator output interacts with an external flow.

[§]Flow control is used throughout in preference to active flow control. A literature study reveals two different definitions of active flow control, both of which have validity. In the first, *active* refers to energy input to the system, such as use of a fluidic jet as opposed to a *passive* vane vortex generator, which alters the system without additional input. In the second definition, *active* refers to the use of the technology within a feedback control system, in that operation is in reaction to a sensor input. The use of FC allows wider discussion and the avoidance of confusion.

Table 2 Characteristics of flow control actuators

Actuator type	Actuator transduction	Topology	Mechanism	Typical application
Air jet actuator [7] — 45° skewed, 200 µm dia. hole in 500 µm thick metal/glass plate; Pulsed jet, 200 - 300 m/s, 5-50% duty cycle; Wetted surface; Pressurised supply (30-80 kPa); PZT cantilever actuator, 50-100 µm displacement, 0 – 500 Hz frequency	Fluidic	Hole	Injection of spatially periodic streamwise vortices	Boundary-layer shape-factor reduction → separation control (high authority)
Synthetic jet actuator [3] — Synthetic jet; Wetted surface; Orifice; Chamber; Diaphragm motion; Diaphragm + PZT patch	Electromechanical-fluidic	Hole	Injection of spatially periodic streamwise vortices	Boundary-layer shape-factor reduction → separation control (high authority)
Membrane actuator [8] — Wetted surface; Membrane slices; Spacer; Piezoceramic element; Support spacer; Substrate; 5 mm; EADS IW-SI	Electromechanical-fluidic	Surface (flow acceleration normal to surface)	Induction of wavelike disturbances	Attenuation of TS waves → laminar–turbulent transition control (low authority)
Plasma actuator [9] — AC HV; Plasma; Wetted surface; Dielectric	Electrofluidic	Surface (flow acceleration tangential to surface)	Induction of spanwise flow oscillations	Breakup of turbulent streaks → skin-friction drag reduction (low authority)

In quantitative terms, the typical application of an FC system can be defined according to the actuator authority, which is based on the ratio of actuator output velocity to the local freestream velocity. *High authority* implies a velocity ratio of around 1, as required for flow separation control applications; *low authority* is defined by a velocity ratio $\ll 1$, as used for transition control and skin-friction drag reduction.

1. Air Jet Actuator

Air jet actuators comprise a class of devices that impart control through injection of high-momentum fluid into an external flow. A distinction may be made between high-authority blowing systems that seek to directly modify the circulation round a lifting body, usually though tangential injection and low-authority blowing systems that seek to reduce the effects of flow separation by enhancing boundary-layer mixing. The present study focuses on the use of pulsed air jet vortex generators or pulsed jet actuators (PJAs) [10]. Data used here are from those given by Warsop et al. [7]. The actuator device is designed to generate streamwise vortices in the boundary layer, with a high-velocity (200–300 m/s) jet of air modulated by operation of a piezoelectric microvalve. The energy efficiency of the air jet actuator is estimated to be around 40%, with most of the losses due to the sudden contraction experienced by the flow moving into the actuator plenum [11].

2. Synthetic Jet Actuator

SJAs are a subset of air jet actuators that use an oscillating mechanical element in a cavity to produce a net momentum flux in an external flow by a process similar to acoustic streaming [12–14]. Like air jet actuators, SJAs seek to control flow separation by enhancing boundary-layer mixing. Example applications of SJA separation control include airfoils and bluff bodies [15,16]. Current-generation SJAs driven by commercial polycrystalline piezoelectric (PZT) diaphragms can achieve reasonably high levels of authority (peak velocity of 150 m/s), with an electrical-to-fluidic power-conversion efficiency of around 10% [3]. Polycrystalline PZT has an electrical-to-mechanical energy conversion efficiency of around 40%, whereas single-crystal PZT has an equivalent efficiency of 80% [17]. Thus, it could be expected that actuator efficiency and authority could be doubled by use of bespoke single-crystal PZT diaphragms in the existing actuator designs.

3. Membrane Actuator

As an alternative configuration to the SJA, the oscillating mechanical element can be a flexible part of the wetted surface, leading to the concept of an active surface or membrane actuator [8,18,19]. The impedance mismatch at the actuator–air interface typically limits the achievable peak velocity output to a few meters per second for practical devices. However, for applications such as transition control, the required actuator velocity is only a few meters per second even at cruise Mach numbers; low-velocity disturbances are required to damp out the Tollmien–Schlichting (TS) waves. Therefore, the low authority of integral surface devices in absolute terms may not be an issue.

Methods of actuating the membrane include mechanical displacement via the use of a loudspeaker and connecting rod [19,20] and fluidic displacement via a pressurized air chamber [21]. The former requires high maintenance and is unrealistic for practical aircraft application, while the latter requires a separate air supply and ducting. A MEMS-based device [8] offers a viable alternative and is used as the reference membrane actuator in this study. The device consists of a surface silicon membrane that amplifies the displacement generated by a piezoceramic disc. The PZT material has an electromechanical coupling factor of 0.7. With transmission losses, a power-conversion efficiency of 60% can be expected. It has been shown that the actuator is capable of influencing TS-wave-specific frequencies between 2.5 and 7.4 kHz at Mach 0.33 to delay transition [22].

4. Plasma Actuator

These devices produce fluidic actuation by ionization and subsequent acceleration of the air local to the actuator. This
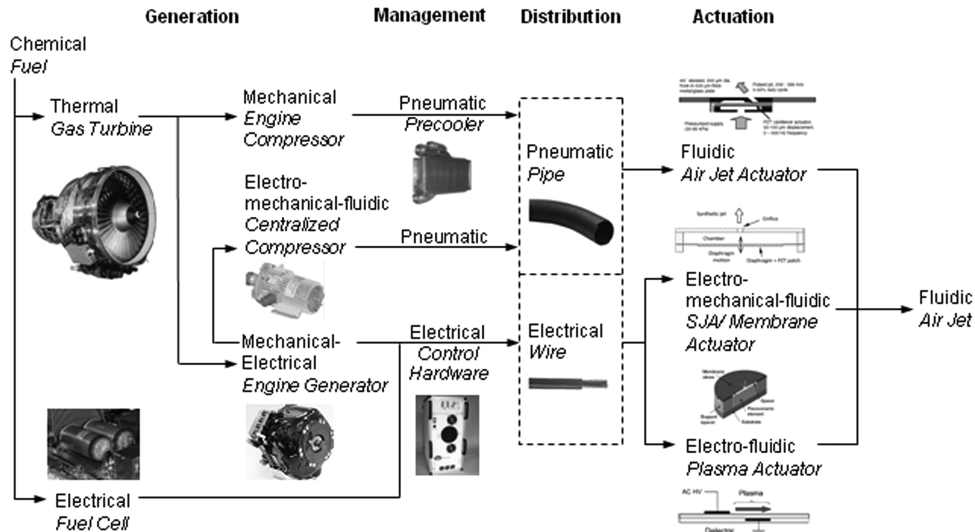
Fig. 1   Flow control systems architectures.

transduction process tends to be very inefficient, e.g., less than 0.1% electrical-to-fluidic energy conversion efficiency [9], with most of the supplied energy dissipated as heat as a result of the ionization process, rather than fluidic kinetic energy. In practice, actuator authority is relatively low: e.g., peak velocities of the order of a few meters per second. This makes plasma actuators a potential candidate technology for applications such as turbulent skin-friction drag reduction. Previous work has shown that surface plasma actuators applied in a turbulent boundary layer are capable of achieving drag reductions of up to 45% [23].

Plasma actuators have a unique advantage in that the transduction process requires no moving parts, which is significant from a maintenance point of view. Additionally, the actuators can be manufactured to be very thin, meaning that retrofit on existing aircraft skins is possible without major structural redesign. Moreau [9] provides a recent review of the literature on plasma actuators. The reference actuator considered is the surface dielectric barrier discharge (DBD) plasma actuator [24,25], which consists of two thin aluminum-foil electrodes flush-mounted across a Plexiglas (polymethyl methacrylate) dielectric layer.

C.   Power Distribution Systems

A true appreciation of the costs of a proposed FC actuator can only be gained by considering how energy supply to the actuator may be achieved within the framework of the aircraft's existing power systems architecture. Figure 1 shows the different energy pathways available for the range of FC technologies considered. The domain of interest covers the overall process of converting chemical energy from fuel into useful fluid power delivered by an FC actuator. Note that the gas turbine power plants may provide a source of compressed air via the bleed system in addition to electrical power via the integrated-drive generators (IDGs). A third possible storage and initial transduction mechanism is the use of fuel cells (either alone or in conjunction with a gas turbine in a hybrid system) for electrical power generation. Although this has not yet been implemented on a production aircraft, the use of such technology in order to replace the auxiliary power unit (APU) in future designs has been considered, with the benefit that water produced as a waste product may be used by the cabin systems [26].

The key system in terms of overall aircraft design is the distribution system, which connects the generation system to the actuator system. The distribution system may be pneumatic, electric, or some combination of the two. It is worth noting that power distribution systems will already be present on the aircraft, and these will give an indication of the likely system design parameters and certification requirements for the FC distribution system and the possibility of deriving synergistic benefits from its shared use.

Pneumatic distribution gives rise to direct bleed-based flow control, in which compressed air can be used to directly power air jet actuators. Hot bleed air piped from the engine offtake requires power management in the form of precooling before passage to the actuator plenums.

Electric distribution is required for SJAs, membrane actuators, and plasma actuators. Before electrical power can be distributed from the IDG to the actuators, it needs to be regulated, conditioned, and, if necessary, converted. This is the function of the power management system, of which a detailed overview is given in [27]. The IDG for an Airbus A320 supplies 115 VAC, 400 Hz, three-phase power. The advantage of running the electrical system at 400 Hz rather than 50/60 Hz is that the power generation systems are smaller and lighter. As a result, FC actuator systems electronics must either be designed to operate with a 400 Hz supply or the power must be converted to low-frequency, single-phase supply. While many aircraft electrical loads can run directly from high-frequency three-phase supply, FC actuators will require dedicated power electronics. In this study, the power management system comprises the following:

1) Generator control unit (GCU) regulates supply voltage and frequency.

2) Electronic load control unit (ELCU) are trip devices that provide electrical load protection.

3) Transformer rectifier unit (TRU) converts three-phase 115 VAC to 28 VDC for FC electronics.

4) Power amplifiers and high-voltage (HV) power transformers.

An alternative is a hybrid approach that uses both electric and pneumatic distribution. This solution uses one or more electrically driven air compressors to generate compressed air locally to the FC actuators. The actuators themselves are identical to those considered for pneumatic systems (i.e., air jet actuators). The advantage over native pneumatic systems is that engine bleed air is not required, and therefore it may be possible to provide the required flow control effectiveness at low engine throttle settings, assuming that generator power is available.

It may be argued that the length and, therefore, mass of piping required in the hybrid approach may be reduced by using several electrical compressors to source air locally to the actuators, rather than a single centralized compressor. This advantage would only come to fruition if (under the assumption that the relative mass costs are less for electrical distribution than for pneumatic distribution) the piping is eliminated completely by performing transduction to fluidic power at the point of actuation: i.e., equipping each air jet actuator with its own compressor for air supply. This architecture would be similar to the distributed electromechanical-fluidic (EMF) and electrofluidic architectures associated with SJAs/membrane actuators and plasma actuators, respectively. The problem with this approach, however, is that, in common with electrical machinery,

Table 3   Comparison of compressor specifications at different scale

Size	Mass flow, g/s	Mechanical efficiency	Actuators per compressor[a]
Microscale [28] 8mm diameter	0.36	~5%	7
Mesoscale [29] 25mm diameter	2.4	~50%	50
Macroscale[b] 200mm diameter	53	~85%	1000

[a]Example application is for an A320 aircraft trailing-edge flap (full-span) separation control (2000 actuators; 100 g/s mass flow rate).
[b]Data available online at http://www.eatonaerospaceltd.com/air/Resources/044_1_BoostCompressor.pdf [retrieved 5 December 2009].

Table 4   FC systems architecture ID

ID	Generation	Distribution	Actuator
1	Engine bleed	Pneumatic	Air jet actuator
2	Electrical air compressor	Pneumatic	Air jet actuator
3	Electrical generator	Electric	Synthetic jet actuator
4	Electrical generator	Electric	Membrane actuator
5	Electrical generator	Electric	Plasma actuator

compressor mechanical efficiency scales with physical size, as shown in Table 3. Efficiency is approximately 5% at the scale required to use a high compressor-to-actuator ratio, compared to 85% by using a centralized macroscale compressor. The efficiency of using a compressor at microscale is approximately half of that associated with SJAs for high-authority flow control. For this reason, the hybrid architecture in the present study is considered in terms of a single centralized electrical air compressor.

D.   Section Summary

From this work it is possible to identify five distinct FC systems architectures, as summarized in Table 4. For simplicity, each architecture is referred to by the ID number hereafter.

III.   Research Methodology

### A.   System Modeling Approach Requirements

The type of model used has a significant effect on the type of questions that the model can be used to answer. A requirement of this work was that the model could be used to understand the effect of using different FC architectures on the overall system mass. This lead to the choice of a low-order, largely physics-based, modeling approach that is not necessarily very accurate, but is fast and transparent [3]. This approach is sufficient to make informed choices between competing architectures for a given application, with the expectation that this choice is followed up with more engineering analysis using higher-order models at a later stage.

B.   Flow Control System Mass Model

The mass model used for the present work is illustrated by the schematic in Fig. 2. The key model inputs are related to system hardware, system energy usage, and aircraft parameters. The model mathematical structure is defined in Eq. (1). The overall FC systems mass cost is made up of the sum of the mass cost of the FC system hardware and the mass cost of the energy used by the system. To produce a scalable model, an assumption is made that mass of cost of the hardware is proportional to the power flowing through the system. This means that generation, management distribution, and actuation systems are defined by *power-specific masses* m_w, with units of kg/kW. The energy-usage term is the mass of fuel used to supply the required power for the duration of operation of the FC system, as calculated from the power-specific fuel consumption of the generator system, $\dot{m}_{Wg}$:

$$m = \frac{W_F}{\eta}[\Sigma m_W(\eta) + \dot{m}_{Wg}\Delta t] \qquad (1)$$

where W_F represents the fluidic output power of the FC system from an array of FC actuators, and η is the overall power efficiency of that system. Changing power efficiency has two different effects in the mass model. The primary effect is that by increasing efficiency, the overall power flow through the system is reduced [first term on the right-hand side (RHS) in Eq. (1)], and everything else remaining equal, the overall system mass decreases. However, it is important to understand how this efficiency is achieved, since there is typically a tradeoff between system power-specific mass and the efficiency (more power-efficient systems typically require more advanced technology and/or higher specification components that are typically heavier). To account for this, the mass model allows the power-specific masses to be functions of efficiency. To illustrate the
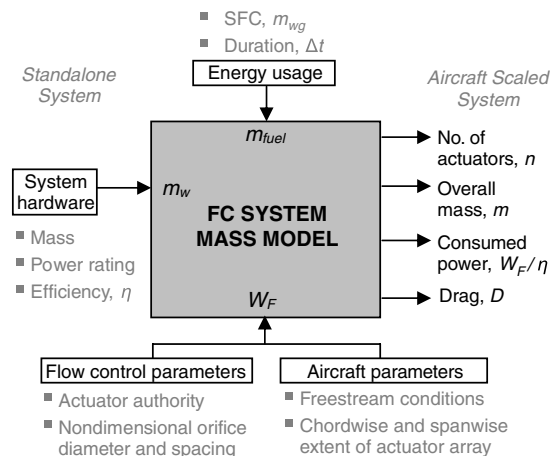
Fig. 2   Schematic of flow control mass model system parameters.
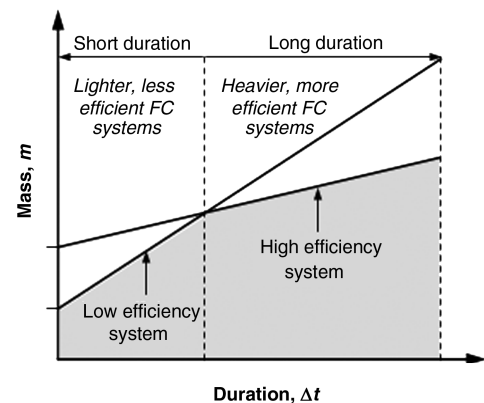
Fig. 3   Illustration of the effect of FC system duration of operation on the design constraints required for minimum mass.
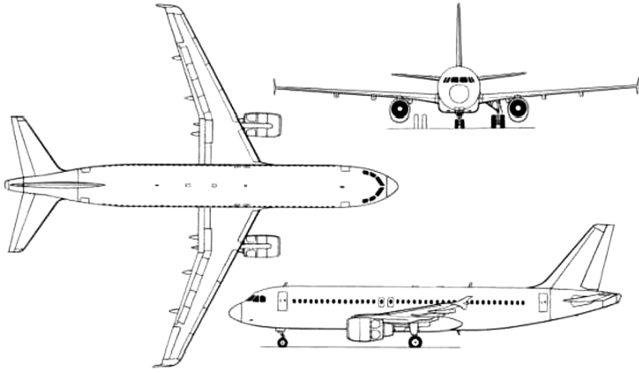
Fig. 4 A320 civil transport aircraft (wing span: 34 m, maximum takeoff mass: 77,100 kg).

implications of this, Fig. 3 shows how the overall mass cost of an FC system varies with the duration of operation of the system for two different power efficiencies. For short-duration operation, minimum mass will typically be driven by using lighter but less efficient systems, whereas for long-duration operation, the minimum-mass solution will be obtained by more efficient but heavier systems.

The FC system duration of operation will have implications for aircraft integration, depending on the portion of the flight mission in which the system is to be operated: e.g., cruise (on-design) or landing/takeoff (typically offdesign). The A320 is a relatively short-range aircraft (2500 nm) and the cruise phase typically represents 60% of the overall flight mission. The major FC application here is cruise drag reduction, which typically requires large numbers of low-authority actuators operating for extended periods of time. As such, *energy optimization* is a key driver for FC systems operating for long durations. The offdesign portion of the flight consists of takeoff and landing and typically represents less than 10% of an overall flight mission. The major FC application is separation control, which typically requires spanwise arrays of high-authority actuators operating for relatively short durations. *Power optimization* is the key driver for such systems.

C. Method

The model introduced and used in [3] for the consideration of a single type of FC actuator has been expanded in this study to include a number of different FC architectures, which requires the consideration of different power sources, distribution systems and actuator technologies described in Sec. II.

The mass, power rating, and efficiency associated with generation, management, and distribution systems hardware were estimated using engineering equipment supplier information in the public domain: e.g., aircraft onboard equipment such as engine electric generators, high-pressure pipes, wiring, and amplifiers (see Appendix A for a more detailed overview). Estimates of the mass, power, and efficiency of the FC actuators were made based on existing laboratory technology. To compare the mass costs for different methods of power distribution, analytical physics of pipe/wire theory are coupled with the engineering constraints of integrating these distribution systems into an A320 aircraft. Detailed derivations of the power distribution theory and assumptions on the systems data and constraints are given in Appendix B.

The systems hardware data are required to evaluate the power-specific mass m_w for each system. The overall power-specific mass permits relative comparisons between different FC systems architectures in terms of systems mass per unit power flow through the system (kg/kW). Power-specific mass is also an input parameter of the mass model (Fig. 2), permitting absolute values of overall system mass and power consumption for different FC systems architectures to be calculated at aircraft full scale.

D. Case-Study Analysis

Case-study analyses for the integration of different FC systems architectures on an A320 aircraft (Fig. 4) wing were carried out for

the purpose of generating understanding of how the flight conditions, FC location, and FC actuator authority affect the overall systems architecture mass and power requirements. Each of these criteria forms inputs to the mass model (Fig. 2). Coupled with these is an additional input for the energy usage associated with the mass of fuel used during operation of the FC system.

Three different flow control case-study scenarios were considered: transition control, skin-friction drag reduction, and separation control. For each of these, one or more FC systems architectures (IDs 2 to 5 in Table 4) were analyzed. The case-study scenarios were developed based around high-speed (cruise) and low-speed (takeoff and landing) flight conditions, as defined in [3]. Chordwise location and spanwise extent of FC actuator arrays for the slat, flap, and wing main element and the related operating duration are also the same as those defined in [3]. The power requirement of a specific FC actuator application depends on the local flow conditions. The actuator layout and equations for the power delivery from each FC actuator system have been derived, as shown in Appendix C.

To place the quantitative outputs of the case studies into context, FC system power consumption is represented as a percentage of the available power supplied from a single-engine generator. The drag cost associated with this power offtake for cruise flight FC applications is represented as a percentage of the A320 cruise drag (estimated from an assumed lift-to-drag ratio of 18 in the clean configuration). Overall mass for FC systems applied on the main element is represented as a percentage of the A320 maximum takeoff weight (MTOW). For slat and flap applications, FC system mass is represented as a percentage of the slat and flap mass, respectively. Slat and flap mass were calculated according to an empirical method [30] coupled with slat and flap configuration data [31], yielding values of 405 and 638 kg, respectively.

A number of important assumptions are made for each case-study analysis.

1) Each case study only takes into account the cost of FC implementation (mass, power consumption, and drag penalty). The impact benefits such as reduced drag and increased maximum lift are not considered.

2) Given that all the present case-study analyses are considered for aircraft wing application, the reference length for distribution lines (i.e., pipes and wires) is based on the A320 wingspan (i.e., 34 m).

3) Redundancy is not accounted for in the present study, in that only single power sources and single lanes of pipes and wires are considered. This will not affect evaluation of the overall system power-specific masses, but it will have an impact on absolute values of overall mass and power consumption subject to the levels of redundancy that would be required to satisfy system certification.

4) Thermal management of electrically powered systems is not accounted for in the present study. However, in some instances, cooling forms an integrated part of the component: e.g., use of heat sinks.

5) Since the energy losses for each FC systems architecture are dominated by losses in the actuator transduction process, it was decided for reasons of simplicity to set all power efficiency terms apart from the actuator efficiency to unity. This is a reasonable assumption given the following:

   a) Aircraft engine generator (IDG) and electrically driven compressor efficiencies are ~85%.

   b) GCU and TRU systems efficiencies are ~95%; power amplifier efficiencies are ~75–80%.

Table 5 Sensitivity analysis of FC system efficiency on overall system mass and power

ID	Overall efficiency	Uncertainty (±10%)	Mass	Power
2	40%	±4%	±12.1%	±10%
3	10%	±1%	±12.2%	±10%
4	60%	±6%	±10.3%	±10%
5	0.1%	±0.01%	±10.2%	±10%

c) Pneumatic pipe and electric cable efficiencies are ∼85% and ∼99%, respectively.

As such, the overall power efficiency of the system, η, which is required to calculate the overall system mass [Eq. (1)], is equal to the actuator efficiency.

6) For architecture 2, pulsed jet operation is considered for the actuation system. The duty cycle, representing the ratio of the jet time on to time off, typically varies between 10 and 50% [7]. A duty cycle of 25% is assumed in this study.

7) For architecture 3, it is assumed that SJAs are capable of achieving sonic output velocities to meet a target velocity ratio of 1 for high-authority separation control applications.

A sensitivity analysis was conducted to investigate the variation of the systems architecture overall mass and power consumption with variation in overall system (actuator) power efficiency. The effect of a 10% uncertainty in overall efficiency was considered for each systems architecture. Table 5 summarizes the sensitivity analysis in terms of the uncertainty generated in overall mass and power consumption for the different architectures. Power consumption scales directly with system efficiency [first term on the RHS in Eq. (1)], and therefore a 10% increase in overall efficiency results in a 10% reduction in the overall power required by the FC system. The overall system mass also reduces by 10%, plus a smaller gain (as shown in Table 5) due to the relatively reduced actuator mass. Recall that the mass model allows power-specific masses to be functions of efficiency; therefore, for this study, the actuator power-specific mass will also vary by 10%. A 10% uncertainty in overall system power efficiency yields variations in the overall system mass between 10 and 12% for the different architectures.

IV. Results

A. Comparison of Different Power Distribution Methods

A comparison of the mass costs of electric and pneumatic distribution as a function of transmitted power is presented in Fig. 5a. Scatter arises in the data from the use of commercially sourced pipes and wires that are only available in discrete sizes. The mass cost of hydraulic distribution is also included for reference, given their extensive use on commercial aircraft.

The results show that there is a large difference in the mass costs associated with different distribution systems, especially for transmission of relatively low power. The mass cost of transmitting 5 kW of power pneumatically is approximately 2 orders of magnitude greater than doing so electrically. This disparity reduces with increasing power transmitted. For example, the ratio of mass costs between electric, hydraulic, and pneumatic distribution at 10 kW is approximately 1:8:35, and at 50 kW, the ratio is 1:3:9. For electric distribution, the mass cost increases with power transmitted. This is due to the weight of the copper wire increasing (for a higher current-carrying capacity) at a faster rate than the power that can be transmitted. Hydraulic and pneumatic distribution show reducing mass cost trends with power transmitted. For pneumatic distribution, wall thickness is fixed (constrained by maximum bleed pressure of the system, as detailed in Appendix B); hence, increasing internal pipe diameter improves power transmission relative to pipe mass.

Variation of distribution efficiency with power transmission type is shown in Fig. 5b. All power losses used to evaluate efficiency are scaled on a distribution length equivalent to the A320 wing span. The efficiencies for all methods of distribution are relatively high and increase with the amount of power transmitted. To transmit high power electrically, a bundle of smaller cables is a more mass-efficient approach than using a single large cable, due to practical issues of insulation and heat transfer. For pneumatic distribution, it is more mass-efficient to use the largest-diameter pipe that can be accommodated in a given volume.

Figure 5c shows the power transmission capacity of various diameter cables and pipes. The ratio of diameters between electric, hydraulic, and pneumatic distribution for 10 kW of power is approximately 1:3:7 and 1:2:4 for 50 kW of power. For the present study, maximum power distribution for a 36 psi pneumatic system is
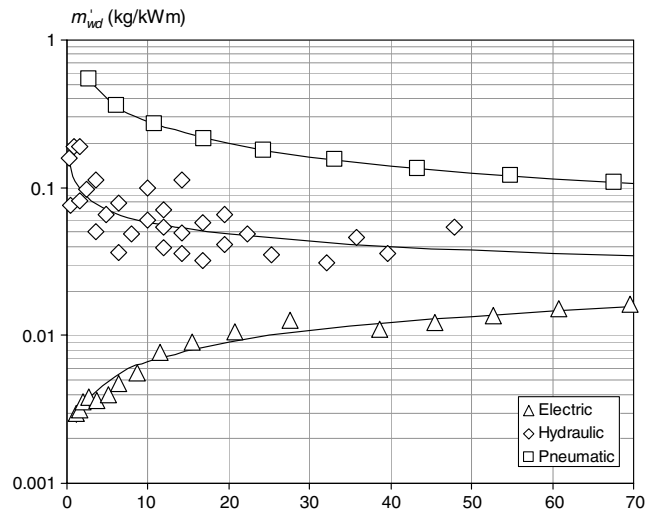
a) Power distribution specific mass per unit length
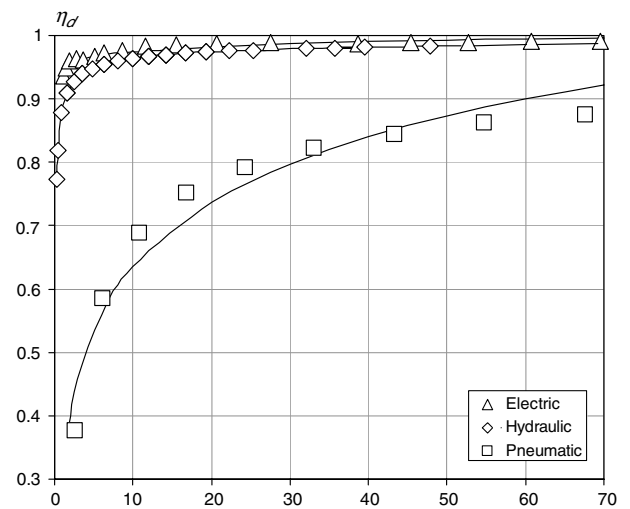
b) Power distribution efficiency
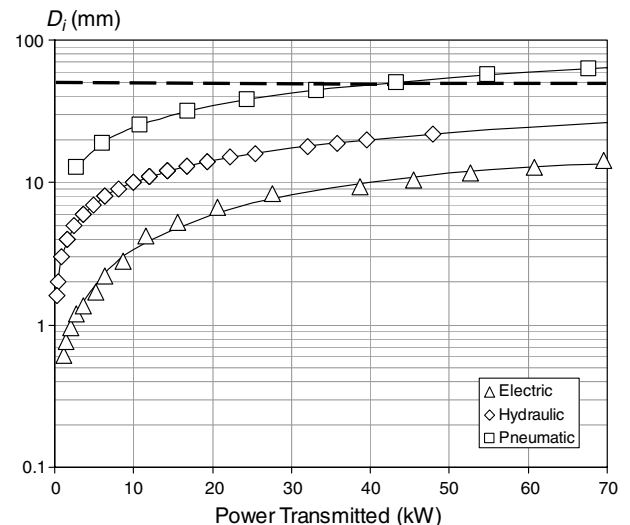
c) Power distribution diameter (dashed line indicates limit of wing LE volume constraint)

Fig. 5   Variation of power distribution characteristics with power transmission.

limited to 50 kW based on the maximum pipe diameter that can be accommodated in the wing leading edge.

Results from this study show that electrical power distribution has clear benefits over pneumatic power distribution for FC applications

in terms of reduced mass, higher overall efficiency, and reduced installed volume for the same power transmitted. These findings are consistent with the perceived move toward the more electric aircraft concept. In particular, decentralization of pneumatic FC systems is in line with future expectations for decentralization of fluidic systems. For example, existing hydraulic systems using a single centralized pump and hydraulic pipes are proposed to be replaced with electric wires and localized pumps in the form of electrohydrostatic actuators close to the point of application: e.g., flight control surfaces [32].

B. Mass Cost Analysis of Flow Control Systems Architectures

A key output of this work is to understand the relative mass costs of power generation, management, distribution, and actuation for the different FC systems architectures. Figure 6 compares the relative system mass costs pertaining to each system architecture (ID defined in Table 4).

The power-specific mass for the native pneumatic system (architecture 1) is estimated to be 5 kg/kW: that is, 5 kg of system hardware required per 1 kW of power flow through that system. To consider the system as fully pneumatic, continuous blowing is assumed such that electrically operated pulsed microvalves need not be considered. Of the overall power-specific mass, approximately 95% of the mass cost is due to distributing air from the engine bleed manifold to the actuator orifice exits. In comparison, the mass costs of generating and managing the bleed air combined with actuation (as continuous blowing is assumed, the actuator elements consist of very simple passive plenum/nozzle devices) is relatively small (5%).

For the hybrid system (architecture 2), the overall power-specific mass cost is approximately 6 kg/kW. As with architecture 1, continuous blowing is assumed and the largest mass cost is incurred in distribution (75% of the total mass cost). The higher overall systems mass cost relative to architecture 1 is due to the power generation system, which encompasses the electrically driven air compressor in addition to the IDG.

Figure 6 shows that the overall power-specific mass for the high-authority EMF system (architecture 3) is 1.3 kg/kW. The smaller cost relative to architectures 1 and 2 is due to the different method of power distribution, i.e., electric, as opposed to pneumatic distri-
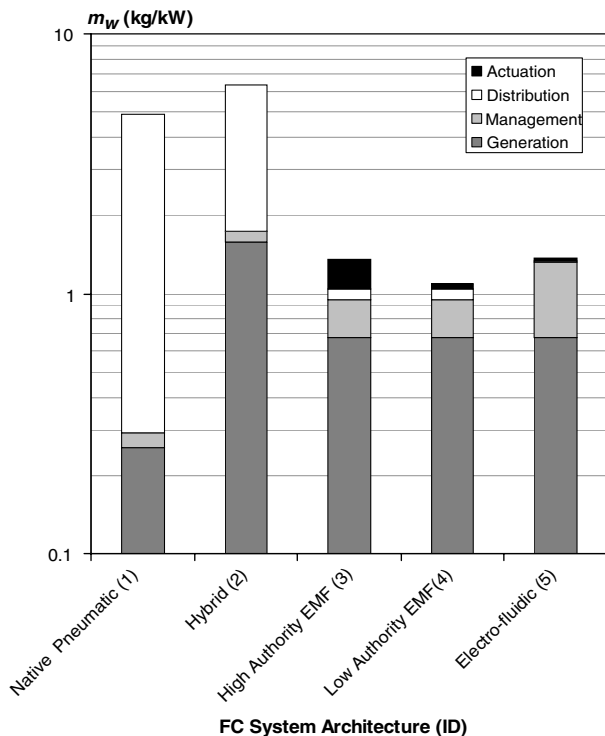
Table 6 Systems architecture 4 power offtake and drag cost for transition control

Application	Power	Drag
Transition control (wing main element) 600 actuators	6 kW (7% IDG)	24 N (0.06% cruise drag)

bution. Approximately 50% of the mass cost is due to the provision of power generation capacity. Power management and actuator systems each contribute 20% of the overall mass cost.

The power-specific mass for the low-authority EMF system (architecture 4) is just over 1 kg/kW (1.1 kg/kW). The system cost is the lowest of all the FC systems architectures considered. Mass costs of generation, management, and distribution are identical to those for architecture 3. By comparison, the mass cost of actuation is smaller due to the combination of a much smaller actuator mass and larger power rating (Appendix A).

Finally, Fig. 6 shows that the overall power-specific mass for the electrofluidic system (architecture 5) is 1.4 kg/kW. This value is comparable to the other electrically based systems architectures (nos. 3 and 4). By comparison, there is a larger mass penalty to pay in power management for transforming the aircraft supply voltage to a higher level. This penalty is offset, however, by the lower mass costs associated with distributing high voltages (tens of kilovolts), since this reduces the current-carrying capacity and hence the mass of wire needed. Figure 6 shows that architecture 5 has a lower distribution cost than architectures 3 and 4. Architecture 5 also has the lowest actuation mass cost by virtue of the thin-sheet nature of the dielectric layer and plasma electrodes.

Existing systems and components inherent to commercial aircraft typically have values of power-specific mass less than 1 kg/kW. Examples for an A320 include the APU at 0.48 kg/kW (Honeywell, GTCP 36–300A, 140 kg, and 291 kW), IDG at 0.68 kg/kW (Sundstrand, 90 kVA, 61 kg, and 90 kW), and fuel boost compressor at 0.91 kg/kW (Eaton, 9.1 kg and 10 kW). Clearly, there is benefit to be gained in reducing the overall power-specific mass of a system in order to reduce absolute mass costs, and existing practice would suggest a target power-specific mass kg/kW $\sim \mathcal{O}(0.1)$ for FC systems. Figure 6 shows that each FC architecture has overall power-specific masses of an order of magnitude greater than existing aircraft systems, although those for architectures 3, 4, and 5 are at unity. On this evidence, electrical power distribution presents the most competitive mass cost option for FC systems architecture integration on civil transport aircraft.

Fig. 6 Comparison of the relative mass costs of power generation, management, distribution, and actuation for various FC systems architectures.
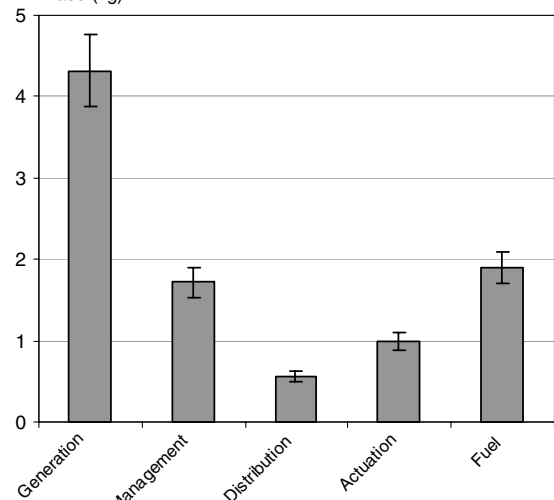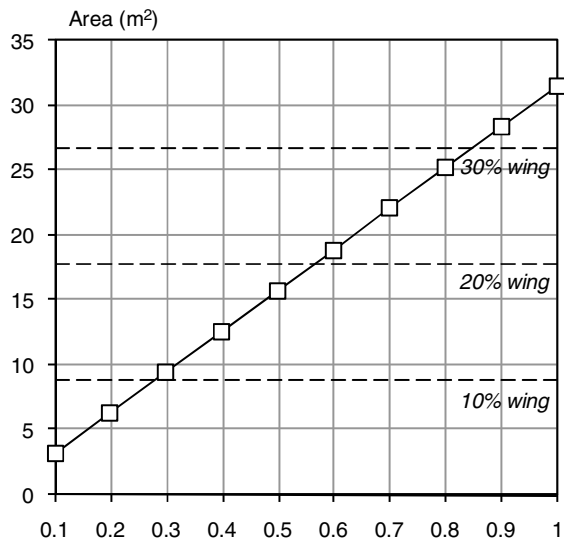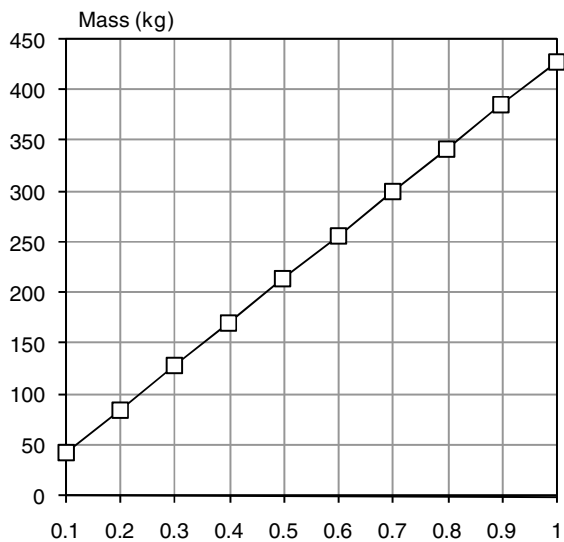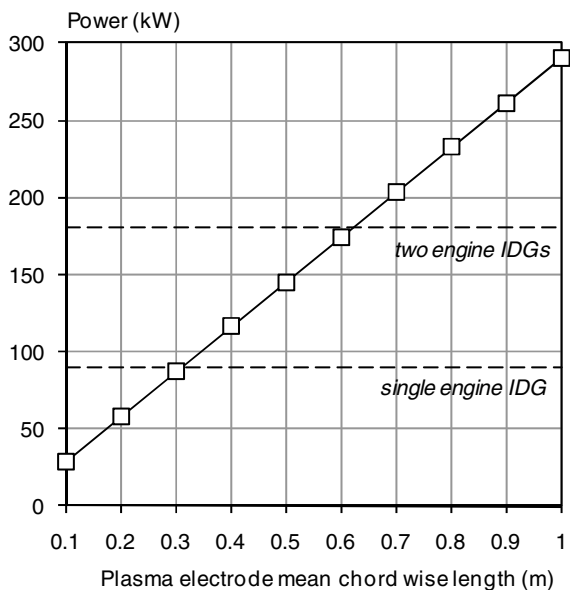

Fig. 7 Mass breakdown of systems architecture 4 for transition control.

a) Plasma electrode area coverage on A320 wing

b) System mass

c) System power consumption

Fig. 8 Characteristics of system architecture 5 as a function of chordwise plasma electrode length.
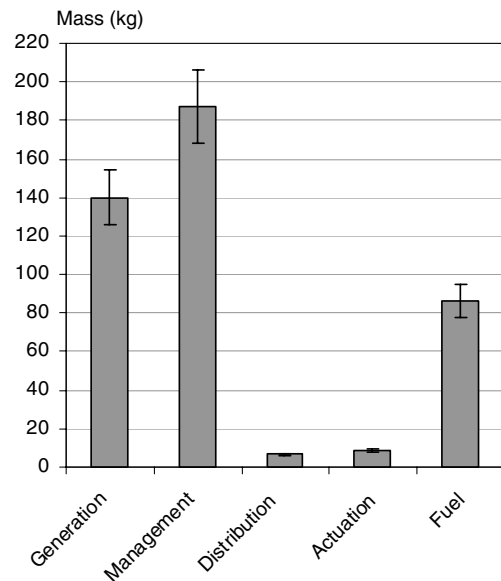

SYSTEMS ARCHITECTURE MASS: ~430kg (0.55% MTOW)

Fig. 9 Mass breakdown of systems architecture 5 for skin-friction drag reduction.

C. A320 Flow Control Case Studies

1. Overview

Results of three different FC case-study scenarios are presented in each of the subsequent sections. Mass breakdown and power offtake of the systems architectures are presented for each case. In addition, drag costs associated with the system power offtake for cruise flight FC applications (transition control and skin-friction drag reduction) are included.

2. Laminar–Turbulent Transition Control: Systems Architecture 4

Figure 7 shows the mass breakdown of systems architecture 4 for transition control via the use of membrane actuators. The total systems architecture mass is approximately 10 kg, which is equivalent to 0.01% of A320 MTOW. One-fifth of this is taken up by the fuel mass required for the duration of operation of the FC system.

Table 6 shows the associated systems architecture power offtake and drag cost. The drag cost establishes the minimum performance benefit necessary from the FC actuators in order for the overall systems architecture to break even: i.e., the point at which further improvements in performance can start to have a positive effect on the overall aircraft. Power offtake is equivalent to 6 kW or 7% of power supplied from an IDG off a single engine. The drag cost is 24 N or 0.06% of the A320 cruise drag.

A point to note is that the A320 wing is a swept wing with crossflow (CF), and Tollmien–Schlichtingg (TS) waves dominated transition. Additionally, the transition location for this (turbulent) wing occurs at approximately 5% of the chord length. Therefore, successful application of this system would realistically require operation on a low-sweep (laminar) wing or operation on the existing swept wing with suction at the wing leading edge to suppress CF instabilities [16]. The latter, of course, would bring in additional requirements for vacuum pumps and pneumatic pipes.

3. Turbulent Skin-Friction Drag Reduction: Systems Architecture 5

Figure 8 shows the actuator surface area coverage, system mass, and power consumption as a function of the mean chordwise length

Table 7 Systems architecture 5 power offtake and drag cost for skin-friction drag reduction

Application	Power	Drag
Drag reduction (wing main element) 750 actuators	291 kW (323% IDG)	1097 N (2.6% cruise drag)

SYSTEMS ARCHITECTURE MASS:
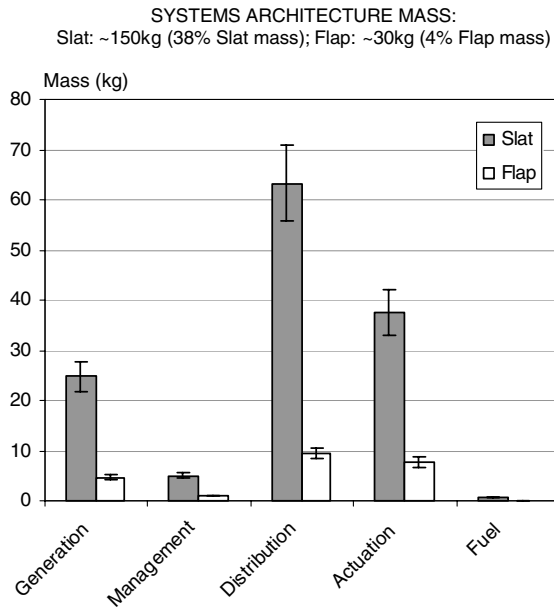Slat: ~150kg (38% Slat mass); Flap: ~30kg (4% Flap mass)

Fig. 10 Mass breakdown of systems architecture 2 for separation control at the slat and flap.

of the plasma electrode actuator array. There is some uncertainty of the streamwise (chordwise) extent over which the plasma electrodes should be applied. In essence, the plasma actuator behaves as an active riblet, and therefore the application of plasma actuators can be considered similar to that of riblets on the A320 in the late 1980s and early 1990s.¶

The geometry of a practical plasma actuator is defined in detail in Appendix C. Figure 8a shows that an array of plasma actuators (750 in total), each with a mean chordwise electrode length of 1 m, would cover approximately 32% of the A320 wing upper surface. This level of coverage equates to a total system mass of 429 kg (Fig. 8b). The power consumption associated with this area coverage is in excess of what can be provided on an A320. For a 1 m mean chordwise electrode length, the power consumption is almost 300 kW (Fig. 8c), which is equivalent to the power supplied from three IDGs.

Figure 9 shows the mass breakdown of systems architecture 5 for skin-friction drag reduction using plasma actuators with a 1 m chordwise electrode length. The total systems architecture mass is approximately 430 kg, equivalent to 0.55% MTOW. This system mass is split almost evenly between power generation and management systems. In addition, there is a high fuel cost (~85 kg) associated with the operation of this system. The high systems mass cost is due to the inefficient transduction process relative to other actuator technologies (plasma actuators with 0.1% electrical-to-fluidic energy conversion efficiency).

Table 7 shows the associated systems architecture power offtake and drag cost. Power offtake is equivalent to 291 kW or 323% of power supplied from a single IDG, and the drag cost is 1097 N or 2.6% of cruise drag.

4. Separation Control: Systems Architectures 2 & 3

Figure 10 shows the mass breakdown of systems architecture 2 for separation control via the use of pulsed air jet actuators. Mass costs are considered for slat and flap FC applications. Total systems architecture mass for the slat is 150 kg, equivalent to 38% of the A320 slat mass. The systems architecture mass for the flap is 30 kg, equivalent to 4% of the A320 flap mass. For both applications, the major contributor in mass costs is power distribution, which represents at least 40% of the overall systems architecture mass.

Table 8 shows the associated systems architecture power offtake for both applications. Power offtake is equivalent to 19 kW or 21% of

¶Private communication, K.-S. Choi, University of Nottingham, 2010.

Table 8 Systems architecture 2 power offtake for separation control

Application	Power
Separation control (slat) 6400 actuators	19 kW (21% IDG)
Separation control (flap) 2000 actuators	4 kW (4% IDG)

IDG power at the slat and 4 kW or 4% of IDG power at the flap. The difference in power costs between slat and flap applications is due to the local actuator jet velocity requirements: leading-edge (LE) slat application requires approximately double the jet velocity of the trailing-edge flap (TE) application. Accordingly, the difference in systems mass costs scales with the difference in power costs.

Figure 11 shows the mass breakdown of systems architecture 3 for separation control via the use of synthetic jet actuators. Total systems architecture mass for the slat application is 120 kg or 29% of slat mass. The systems architecture mass for the flap application is 20 kg or 3% of flap mass. The overall systems mass cost for architecture 3 is 20–30% lower than architecture 2. This difference is largely due to the different power distribution systems used. Slat separation control requires 60 kg of pipes for architecture 2, compared to just 7 kg of cables for architecture 3. Flap separation control requires 9 kg of pipes for architecture 2, compared to 1 kg of cables for architecture 3.

Table 9 shows systems power offtake associated with architecture 3. The power required for the slat is 86 kW or 96% of power supplied from a single IDG and for the flap is 16 kW or 17% of IDG power. These results show that a single-engine generator would be required to power architecture 3 for slat separation control. The power costs for architecture 3 are at least four times higher than those for architecture 2. Note that the power required for operation of architecture 3 at the flap is comparable to that required for architecture 2 at the slat. The driver for this disparity is the low power-conversion efficiency associated with the transduction process in a SJA (10% efficiency).

5. Overall Flight Mission: All-Electric Flow Control

To present a wider overview of the impact of FC systems architectures on a civil transport aircraft, a typical mission profile of an A320 is considered with integrated FC operation during takeoff, cruise, and landing. Figure 12 shows the mass and power profile of an all-electric-based FC solution. Architecture 3 is operated during takeoff (including initial climb) and landing (including approach) for
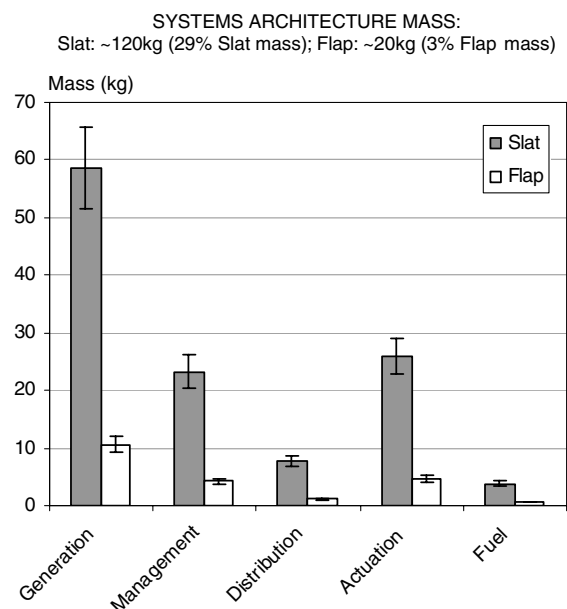
SYSTEMS ARCHITECTURE MASS:
Slat: ~120kg (29% Slat mass); Flap: ~20kg (3% Flap mass)

Fig. 11 Mass breakdown of systems architecture 3 for separation control at the slat and flap.

Table 9 Systems architecture 3 power offtake for separation control

| Application	Power
Separation control (slat) 6400 actuators	86 kW (96% IDG)
Separation control (flap) 2000 actuators	16 kW (17% IDG)

separation control for a total of 10 min. Architectures 4 and 5 are operated during cruise for transition control and skin-friction drag reduction, respectively (68 min each).

The FC mass profile in Fig. 12a shows that the fixed mass of these architectures makes up a combined total of 343 kg, with an additional 50 kg of fuel used to supply the required power during FC operation. Note that the systems mass of architecture 5 assumes a mean electrode chordwise length of 0.5 m, which is equivalent to 18% wing surface area coverage.
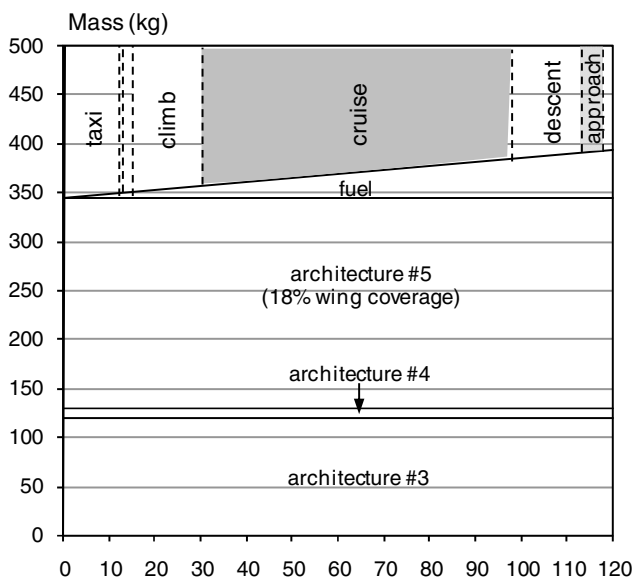
a) Fixed (system) and variable (fuel) FC mass for a typical A320 mission
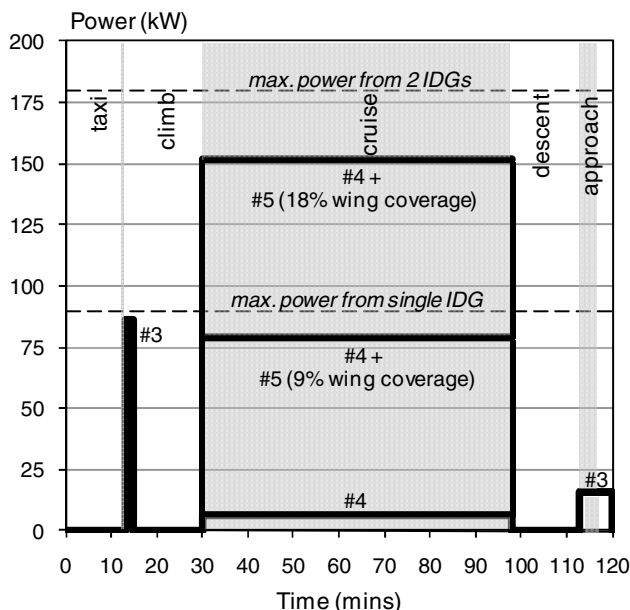
b) FC power profile for a typical A320 mission

Fig. 12 A320 mission using all-electric flow control a) mass profile and b) power profile.

To put this value into context, the total mass is equivalent to 0.6% MTOW or 40% of the combined mass of the slat and flap. The fuel mass required is equivalent to 16 (U.S. liquid) gallons of kerosene. This can be compared to the total amount of aircraft fuel used for the flight mission, as determined from Eq. (2) [33]:

$$E = \frac{HVS}{SMPG} \qquad (2)$$

where E represents energy usage (gallons of fuel), H is the number of airborne hours, V is the average aircraft speed, S is the number of aircraft seats, and SMPG is the seat-miles per gallon. For the 150-seater Airbus A320, which has an average speed of 400 mph and SMPG of 70.2 [33], a 2 h flight consumes 1700 gal of fuel. The fuel used by the FC systems is 1% of the fuel consumed by the aircraft.

The power profile in Fig. 12b illustrates the time-dependent power consumption for FC operation during the flight mission. In this example, the application of architecture 3 is considered solely for LE separation control (slat) during takeoff and for TE separation control (flap) during landing. The power peak during takeoff is close to the maximum available power from a single IDG. Consequently, the provision of power for LE and TE flow control during takeoff would require additional power to be supplied from the second IDG. For a mean plasma electrode chordwise length of 0.25 m for architecture 5 (9% wing area coverage), the power demands for cruise FC applications and takeoff separation control are both comparable.

Given the time-dependent nature of the power profile, it is possible to evaluate total energy usage associated with FC operation. The issue of energy efficiency is a key driver for FC systems operating over long durations, such as cruise flight. The FC energy use during cruise varies from 25 MJ (architecture 4) to 600 MJ (architectures 4 and 5 with 18% wing coverage). In comparison, the total FC energy use during takeoff and landing is 20 MJ. Put into context, the kinetic energy of a fully loaded A320 cruising at 550 mph is equivalent to 2500 MJ. Therefore, FC energy use in cruise varies from 1 to 25% of the aircraft cruise kinetic energy. The upper bound represents a significant portion of the total energy and is due to the relatively inefficient actuators used in architecture 5 for skin-friction drag reduction.

V. Conclusions

This paper has considered the effect of choice of actuator technology and associated power systems architecture on the mass cost of implementing active flow control (FC) systems on civil transport aircraft. The research method employed is based on the use of a simple systems mass model that includes a mass term due to systems hardware (pertaining to generation, management, distribution, and actuation systems) and a mass term due to the system energy usage (mass of fuel used during FC operation).

The study has involved 1) first-principles physical analysis of electric, pneumatic, and hydraulic power distribution systems, combined with 2) collecting hardware data from existing equipment suppliers for the FC systems architectures considered (FC actuator technologies include air jet actuators, synthetic jet actuators, membrane actuators, and plasma actuators), and 3) application of FC systems architectures for various flow control case-study scenarios on an A320 civil transport aircraft.

Specific conclusions from the top-level FC systems architectures study are as follows:

1) A tradeoff exists between system power efficiency and the system hardware mass required to achieve this efficiency. For short-duration operation the solution is driven toward lighter but less efficient systems, whereas for long-duration operation there is benefit in considering heavier but more efficient systems.

2) A sensitivity analysis shows that a 10% variation in the overall power efficiency of an FC systems architecture, which is equivalent to the actuator power efficiency in the present work, will result in a 10% variation in overall power consumption and a 10 to 12% variation in overall system mass, dependent on the specific

architecture. As such, the actuator power efficiency is critical in driving the mass efficiency of the overall system.

3) The mass cost of electric power distribution is shown to be considerably less than that for pneumatic systems (up to 2 orders of magnitude smaller), with added benefits of higher efficiency and smaller volume installation requirements for a given level of power transmission. However, this advantage is reduced by the requirement for relatively heavy electrical power management systems.

4) Systems architectures using power-distributed electromechanical-fluidic actuators with overall power-specific masses of unity, which is similar to the power-specific mass of existing systems inherent to commercial aircraft, are currently the most competitive FC solutions from a mass cost perspective.

Specific conclusions from the A320 case-study analyses for laminar–turbulent transition control (systems architecture 4) are as follows:

1) The total systems architecture mass via the use of a single array of distributed low-authority membrane actuators along the wing main element is approximately 10 kg (0.01% MTOW). The equivalent power offtake is 6 kW (7% of power supplied from a single-engine generator IDG) and the associated drag cost due to this power offtake is 24 N (0.06% A320 cruise drag).

2) The application of this flow control is best suited to a low-sweep (laminar) wing (otherwise, a swept wing with consideration of LE suction to suppress CF instabilities).

Specific conclusions from the A320 case-study analyses for turbulent skin-friction drag reduction (systems architecture 5) are as follows:

1) The total systems architecture mass via the use of a single array of DBD plasma actuators (with mean chordwise electrode length of 1 m) at the wing main element is approximately 430 kg (0.55% MTOW). The equivalent power offtake is 291 kW (323% of power supplied from a single IDG), and the associated drag cost due to this power offtake is 1097 N (2.6% of A320 cruise drag).

2) Maximum power supply from a single IDG is sufficient to support a 0.3 m mean chordwise length of plasma electrode array, equivalent to 11% of the wing surface area.

Specific conclusions from the A320 case-study analyses for separation control (systems architectures 2 and 3) are as follows:

1) FC systems architectures for LE separation control require greater power than for TE applications, due to the greater local velocity at the LE.

2) An array of PJAs (no. 2) consumes less power for LE and TE applications than SJAs (no. 3) for nominally the same effectiveness (21 and 4% of IDG power, compared to 96 and 17%, respectively), due to the greater inefficiency of SJAs.

3) The systems architecture for SJAs confers smaller mass penalties than for PJAs at the LE (29 and 38% of slat mass) and TE (3 and 4% of flap mass), due to the higher mass distribution costs of architecture 2.

4) The provision of an all-electric FC systems architecture for takeoff (LE separation control via SJAs), cruise (transition control via membrane actuators and skin-friction drag reduction via plasma actuators on the main element), and landing (TE separation control via SJAs) for a 2 h A320 flight profile costs 0.6% MTOW in system mass and requires 1% of the aircraft mission fuel.

Appendix A: Flow Control Systems Hardware Data

A summary of the engineering equipment supplier information used to evaluate power-specific masses of hardware for FC systems architectures is shown in Table A1.

Note that calculating the generation power-specific mass for systems architecture 1 requires apportioning the compressor mass as a fraction of the engine dry mass, based on the fraction of bleed air compared to engine core mass flow. Reference data for the applicable engine (CFM56-5B) mass, total engine inlet airflow, and bypass ratio were obtained from [35]. Variations in throttle settings during takeoff and landing will affect the bleed-air mass and hence the effective generation mass. At takeoff power, the maximum permissible bleed extraction from the compressor is 7% of the core airflow [36]. Maximum bleed at landing is assumed to be half of that at takeoff.

Appendix B: Power Distribution Systems

I. Theory

Power is distributed around an aircraft primarily in three ways: electrically, hydraulically, and pneumatically. Traditionally, civil transport aircraft have used all of these methods, with different choices for different service applications. The choice of power distribution will typically depend on the peak power requirement of the application, the available space (volume) between the source and point of application, and the mass cost of distributing power to that application. The following analysis introduces a low-order method for estimating the power-specific mass of electric, hydraulic, and pneumatic power distribution systems for aircraft applications.

For fluidic power distribution (hydraulic and pneumatic), there are two components associated with the power transmitted through a pipe: pressure power W_P [Eq. (B1)] and flow power W_F [Eq. (B2)]:

$$W_P = PUA \qquad (B1)$$

Table A1   Power-specific masses of systems hardware

ID	Generation	Management	Distribution	Actuation
1	CFM6-5B engine compressor 86 kg and 336 kW ($m_{wg} = 0.26$ kg/kW)	Liebherr precooler, 25 kg and 708 kW ($m_{wm} = 0.035$ kg/kW)	SIL2-2001[a] silicone-coated fiberglass duct, 250 kPa; 0.33 kg/s; 43 kW ($m'_{wd} = 0.066$ kg/kWm)	Piezoelectric cantilever-based microvalve [7] 0.1 g and 50 mW ($m_{wa} = 2.0$ kg/kW)
2	Sundstrand 90 kVA engine generator 61 kg and 90 kW ($m_{wg} = 0.68$ kg/kW) Eaton boost compressor 9.1 kg and 10 kW ($m_{wg} = 0.91$ kg/kW)	IPS CV03-75D-1A GCU (including TRU), 9 kg and 75 kW ($m_{wm} = 0.12$ kg/kW) Leach International WE-X9YN ELCU 2.2 kg; 92 kW ($m_{wm} = 0.02$ kg/kW)	SIL2-2001[a] silicone-coated fiberglass duct, 250 kPa; 0.33 kg/s; 43 kW ($m'_{wd} = 0.066$ kg/kWm)	Piezoelectric cantilever-based microvalve [7] 0.1 g and 50 mW ($m_{wa} = 2.0$ kg/kW)
3	Sundstrand 90 kVA engine generator 61 kg and 90 kW ($m_{wg} = 0.68$ kg/kW)	No. 2 and Apex amplifier (PA52 and EK27), 0.5 kg and 4 kW ($m_{wm} = 0.13$ kg/kW)	MIL-W-22759/34[b] XL-ETFE[c] cable, 600 V (single end) ($m'_{wd} = 3 \times 10^{-3}$ kg/kWm)	Synthetic jet actuator [3] 1.5 g and 5 W ($m_{wa} = 0.30$ kg/kW)
4	Sundstrand 90 kVA engine generator 61 kg and 90 kW ($m_{wg} = 0.68$ kg/kW)	No. 2 and Apex amplifier (PA52 and EK27), 0.5 kg and 4 kW ($m_{wm} = 0.13$ kg/kW)	MIL-W-22759/34[b] XL-ETFE[c] cable, 600 V (single end) ($m'_{wd} = 3 \times 10^{-3}$ kg/kWm)	Membrane actuator [8] 0.7 g and 4.6 W ($m_{wa} = 0.15$ kg/kW)
5	Sundstrand 90 kVA engine generator 61 kg and 90 kW ($m_{wg} = 0.68$ kg/kW)	No. 2 + Westinghouse HV transformer [34] (100 kV/1.5 A), 75 kg and 1.5 kW ($m_{wm} = 0.5$ kg/kW)	Belden CD 13209[d] 25 kV extra high tension cable (single end); 3 A; 75 kW $m'_{wd} = 7 \times 10^{-4}$ kg/kWm)	Plasma DBD actuator [9] 4.6 g and 0.15 kW/m ($m_{wa} = 0.03$ kg/kW)

[a]Data available online at http://www.flexfab.com/Brochures/Aerospace%20Brochure.pdf [retrieved 21 Aug. 2010].
[b]Data available online at http://www.wirefacts.com/MIL-W-2275934.php [retrieved 15 May 2009].
[c]Cross-linked ethylene-tetrafluoroethylene.
[d]Data available online at http://www.farnell.com/datasheets/80469.pdf [retrieved 21 Aug. 2010].

Table B1　Aircraft power distribution data based on an A320

	Electric	Hydraulic	Pneumatic
Specification	XL-ETFE and tin-plated copper wire	Stainless steel tube	Silicone-coated fiberglass hose
System rating	115 VAC	3000 psi, 140 l/ min	36 psi; 4 lb/s
Transmission medium	Copper	AeroShell Fluid 71	Bleed air
Density of transmission medium	8900 kg/m^3	880 kg/m^3	1.9 kg/m^3
Kinematic viscosity	——	14 mm^2/s	10 mm^2/s
Transmission velocity	——	6 m/s	86 m/s ($M = 0.2$)

$$W_F = \frac{1}{2}\rho U^3 A \qquad (B2)$$

where P is the fluidic pressure, U is the pipe flow velocity, A is the pipe cross-sectional area (based on the internal diameter), and ρ is the fluid density. For power distribution applications, the pressure power is typically much larger than the flow power, and therefore the latter can be ignored. For a given pipe material with a given mass per unit length m_d/L, the power-specific mass per unit length m'_{wd} or the mass cost required to deliver a unit of power along a unit length of pipe can be defined as

$$m'_{wd} = \frac{W_P}{(m_d/L)} \qquad (B3)$$

For a given pipe length, the distribution efficiency η_d can be determined from the power loss based on the pressure drop down the pipe. The pressure drop due to friction, Δp, for flow in a pipe of any uniform cross section is given by Eq. (B4):

$$\Delta P = 4f\frac{L}{D_i}1/2\rho U^2 \qquad (B4)$$

The equivalent power drop and distribution efficiency are given in Eqs. (B5) and (B6), respectively:

$$W_{\Delta p} = \Delta PUA \qquad (B5)$$

$$\eta_d = \frac{W_P - W_{\Delta P}}{W_P} \qquad (B6)$$

where f is the friction factor, L is the pipe length, and D_i is the internal diameter of the pipe. An approximation for the friction factor based on the Prandtl law for smooth pipes [37] is given by Eq. (B7):

$$f = [1.56 \ell_n(Re/7)]^{-2} \qquad 10^4 < Re < 10^7 \qquad (B7)$$

For electrical power distribution, the electrical power W_E transmitted through a wire is given by Eq. (B8):

$$W_E = VI \qquad (B8)$$

where V is the wire voltage and I the current passing through the wire. A given cable with a mass per unit length (based on the combined mass of the wire and insulation) will allow the power-specific mass per unit length to be determined according to Eq. (B3).

For a given wire length, the distribution efficiency η_d can be determined from the power loss based on the voltage drop down the wire (analogous to the pressure drop down a pipe). The voltage drop due to resistance, ΔV, down a wire is given by Eq. (B9):

$$\Delta V = IR \qquad (B9)$$

The equivalent power drop and efficiency are given in Eqs. (B10) and (B11), respectively:

$$W_{\Delta V} = I^2 R \qquad (B10)$$

$$\eta_d = \frac{W_E - W_{\Delta V}}{W_E} \qquad (B11)$$

where R is the electrical resistance of the wire. Wire manufacturers typically quote the resistance for a given conducting material in terms of a resistance per unit length R/L.

II.　Engineering Data and Constraints

Placed within the engineering constraints of a given aircraft, the derived power-specific masses and efficiencies can be compared for each method of power distribution. Table B1 lists the specifications and operating conditions associated with electric, hydraulic, and pneumatic distribution systems on an Airbus A320.

Electric assumptions are as follows:

1) Primary power generation is from two 90 kVA (115 VAC, 400 Hz, three-phase) engine-driven IDGs.

2) For a nominal system voltage of 115 VAC, the maximum allowable voltage drop that may occur between the power bus and any unit of electric equipment is 4 V for continuous operation and 8 V for intermittent operation [38].

3) To account for inhibited heat dissipation when multiple conductors are bundled together, as is the case for standard wiring, the maximum current-carrying capacity is reduced to 80% for 2–5 conductors, 70% for 6–15 conductors, and 50% for 16–30 conductors [38].

4) Range of wire diameters D_i and insulation thickness WT are $1 \leq D_i \leq 14$ mm and $0.3 \leq$ WT ≤ 1.3 mm.

Hydraulic assumptions are as follows:

1) Pressure rating for the system is constrained by the engine-driven pumps and electric pumps, which supply 3000 psi. The maximum deliverable flow rate is 140 liter/ min (by the engine-driven pumps in the Green system).

2) Flow velocity in the pipes is limited to 6 m/s based on industrial practice.**

3) Range of tube diameters, D_i and wall thickness, WT are $2 \leq D_i \leq 22$ mm and $0.5 \leq$ WT ≤ 4.0 mm.

Pneumatic assumptions are as follows:

1) The pressure rating of the system depends on the bleed pressure of the engine offtake, which is subject to the aircraft flight condition. System rating for the A320 is assumed to be the same as that quoted by McLean et al. [39] for the similar CFM56-7B power plant on the Boeing 737-700. At the landing flight condition, the bleed pressure is 36 psi at a flow rate of 4 lb/s. Corresponding bleed temperature is approximately 460 K [40].

2) Flow velocity in the hose is limited to a Mach number of 0.2 based on industrial practice.

3) Range of hose diameters D_i and wall thickness WT are $25 \leq D_i \leq 68$ mm and WT $= 1.8$ mm for all hose diameters.

In addition to the above constraints, volume constraints within the aircraft must be taken into consideration. The aircraft wing is the major end application for FC systems, and for the present study, volume is constrained by what can be accommodated in the wing LE. Based on evidence from pneumatic LE anti-ice systems, it is estimated that the maximum diameter of pipe or cable for power distribution should not exceed 50 mm.

Appendix C: Layout and Power Delivery of Actuator Systems

I.　Air Jet Actuators

The fluid mechanics underpinning pneumatic air jet actuator systems is based on empirical data on the performance of momentum injection devices used for separation control applications. This is also applicable for synthetic jet actuators (next section). A simple

---

**Data available online at http://www.hydraulic-supply.com/pdf/1498.pdf [retrieved 21 Aug. 2010].

dimensional analysis of the problem suggests that the interaction of a jet in a crossflow is defined by the following dimensionless parameters.

The ratio of orifice diameter to local boundary-layer height is

$$\Delta = \frac{d}{\delta} \tag{C1}$$

The ratio of actuator spanwise spacing to orifice diameter is

$$\lambda = \frac{l}{d} \tag{C2}$$

The ratio of peak jet velocity to local freestream velocity is

$$V_R = \frac{\hat{U}_j}{U_\infty} \tag{C3}$$

Empirical evidence for fluidic jets suggests that for both effectiveness and efficiency for flow separation control, typical values for the dimensionless parameters in Eqs. (C1–C3) are $\Delta \approx 0.2$ [7], $\lambda \approx 10$ [41], and $V_R \approx 1$ [42,43]. Figure C1a shows the actuator layout, and Fig. C1b shows the required coverage on the wing slat and flap surfaces for separation control.

The mean fluid power delivered by a total of n actuators is, by definition, given by

$$W_F = \tfrac{1}{2} n \rho A \bar{U}_j^3 \tag{C4}$$

where ρ is the jet air density; A is the orifice area, and $\bar{U}_j^3$ is the time average of the cube of the jet velocity. The number n of actuators required for a given boundary-layer height and spanwise extent of array s_A is given by

$$n = \frac{s_A}{\lambda \delta \Delta} \tag{C5}$$

For steady jet operation, $\bar{U}_j = \hat{U}_j$. Therefore, the required fluid power for a given flow control application is given by

$$W_F = \frac{\pi}{4} \frac{V_R^3 \Delta}{\lambda} \frac{1}{2} \rho s_A \delta U_\infty^3 \tag{C6}$$

If the jet is pulsed, a duty cycle τ is included:

$$W_F = \tau \frac{\pi}{4} \frac{V_R^3 \Delta}{\lambda} \frac{1}{2} \rho s_A \delta U_\infty^3 \tag{C7}$$

Mass flow rate and air jet plenum pressure requirements are derived in [44]. The mass flow rate required is given by

$$\dot{m} = \tau \frac{\pi \rho \delta^2}{4} n \Delta^2 V_R U_\infty \tag{C8}$$

The air jet driving pressure is given as

$$(P_{\text{plenum}} - P_0) = \frac{P_0}{k_{\text{jet}}} \left\{ \left[\frac{\gamma - 1}{2} (M_R M_\infty)^2 + 1 \right]^{\frac{\gamma}{\gamma-1}} - 1 \right\} \tag{C9}$$

where P_{plenum} is the plenum pressure, P_0 is the ambient pressure, k_{jet} is the orifice efficiency (equivalent to η), M_R is the ratio of peak jet to local freestream Mach number, M_∞ is the local freestream Mach number, and γ is the gas constant (1.4).

The mass flow rate and air jet plenum pressure can be used to size the distribution line (pipe area A) of pneumatic-based FC systems for a given flow control application, according to

$$A = \frac{\dot{m} R T}{U(P_{\text{plenum}} + P_0)} \tag{C10}$$

where U is the pipe flow velocity, T is the fluid temperature in the pipe, and R is the universal gas constant.
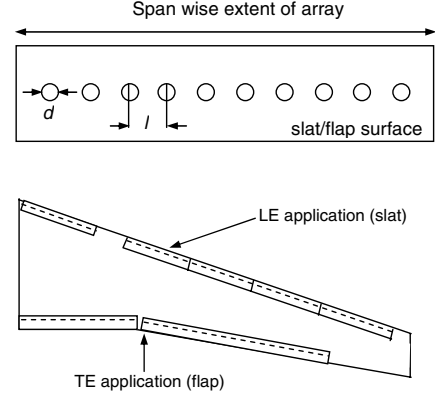

Fig. C1   Air jet actuator configuration: a) array layout and b) slat/flap coverage.

II.   Synthetic Jet Actuators

The actuator layout for SJAs is the same as that given for the air jet actuator array (Fig. C1). Assuming sinusoidal oscillation of the SJA diaphragm, the relationship between the time average jet velocity and peak jet velocity is given by

$$\bar{U}_j^3 = \frac{1}{T} \int_0^T [U_j(t)]^3 \, dt = \frac{5}{16} \hat{U}_j^3 \approx \frac{1}{3} \hat{U}_j^3 \tag{C11}$$

Substitutions of Eqs. (C3) and (C5) into the equation for required power [Eqs. (C3) and (C5)] and use of the expression for the mean cube of the jet velocity [Eq. (C11)] gives the following expression for the required fluid power for a given flow control application:

$$W_F = \frac{\pi}{12} \frac{V_R^3 \Delta}{\lambda} \frac{1}{2} \rho s_A \delta U_\infty^3 \tag{C12}$$

III.   Membrane Actuators

The mean mechanical power delivered by a total of n membrane actuators is, by definition, given by

$$W_F = n F \bar{U}_j \tag{C13}$$

where F is the dynamic force of the active surface, given by

$$F = m \omega^2 a \qquad F = 4\pi^2 f^2 m a \tag{C14}$$

where f, m, and a are the oscillation frequency, mass, and peak-to-peak displacement of the active surface, respectively. Assuming sinusoidal oscillation of the active surface,

$$\bar{U}_j = a 2\pi f \approx \tfrac{1}{3} \hat{U}_j^3 \tag{C15}$$

Substitutions of Eqs. (C3), (C5), and (C14) into the equation for required power [Eq. (C13)] and use of the expression for the mean velocity [Eq. (C15)] gives the following expression for the required output power for a given flow control application:

$$W_F = \frac{1}{27} \frac{V_R^3}{\lambda} \frac{1}{da} m s_A U_\infty^3 \tag{C16}$$

From Eq. (C2), an actuator spacing of $\lambda \approx 10$ is assumed.

IV.   Plasma Actuators

Figure C2a shows a proposed layout for the plasma DBD actuator array for skin-friction drag reduction[††] and Fig. C2b shows the required area coverage on the wing surface.

A single DBD actuator is made up of one air-exposed electrode and one insulated (ground) electrode mounted either side of a dielectric layer. The generation of spanwise flow oscillations for drag

---

[††]Private communication, E. Moreau, University of Poitiers, 2010.
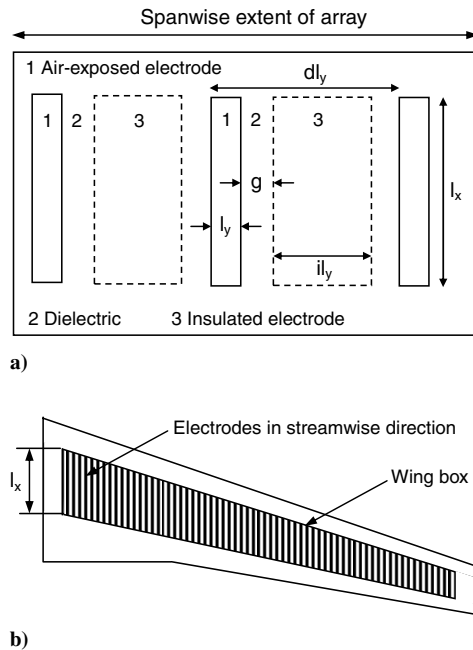
Fig. C2 Plasma DBD actuator configuration: a) array layout and b) wing-box coverage.

reduction requires streamwise electrode alignment. The actuator geometry in Fig. C2a is defined by the electrode streamwise length l_x, the air-exposed electrode spanwise length l_y, the insulated electrode spanwise length il_y, the dielectric layer spanwise length dl_y, and the gap between successive electrodes, g.

It is anticipated that the electrodes have to cover the entire surface over which skin-friction drag reduction is desired, while avoiding areas with high levels of 3-D flow (e.g., leading and trailing edges, wing-fuselage junction, and wing tip). This would equate to a surface area coverage, per wing, of 44.65 m². [‡‡] For the purpose of this study, a mean continuous streamwise electrode deployment of 1 m (l_x) is assumed.

Table C1 confirms the geometry of a plasma actuator for a practical aircraft application.

The kinetic power induced by the plasma is similar to the jet flow displaced through discrete orifices, as associated with the systems described in previous sections. For this reason and according to [9], the kinetic power induced by the electric wind can be derived from Eq. (C4), where $\bar{U}_j$ is the time average of the discharge-induced velocity. The area A is equivalent to the cross section of the plasma, which is the product of the streamwise length of the air-exposed electrode, l_x, and the height of the induced velocity profile, h: i.e.,

$$A = l_x h \qquad (C17)$$

where h can be assumed to be 2 mm (see footnote [††]).

For sinusoidal operation, the peak discharge velocity is related to the time-averaged velocity by Eq. (C11). Note that savings in system power and weight can be achieved by pulsed operation. The ratio of system overall mass (and power consumption) between sinusoidal and pulsed (25% duty cycle) operation is approximately 1.3:1.

For turbulent skin-friction drag reduction, effectiveness requires the actuator velocity output to be of the order of the turbulent friction velocity, which is typically about 5% of the freestream velocity [45]. Hence, $VR = 0.05$ is assumed, which gives $\hat{U}_j \approx 10$ m/s. The total number n of actuators for a given application is

$$n = \frac{s_a}{\lambda l_y} \qquad (C18)$$

where s_a is the spanwise extent of the actuator array along the span of the wing, and λ is the ratio of actuator spanwise spacing (that is, the

Table C1 Plasma actuator geometry for a practical aircraft application

Parameter	Value
l_x	1 m
l_y	2 mm
il_y	36 mm
dl_y	42 mm
g	2 mm

spanwise spacing between successive air-exposed electrodes) to the spanwise length of the air-exposed electrode, l_y. Based on the layout of the actuator array (Fig. C2), $\lambda = 20$. Full-span application on an A320 ($s_a \approx 30$ m) therefore requires a total of 750 actuators (375 per wing).

Substituting Eqs. (2–B4) into Eq. (1) gives

$$W_F = \frac{1}{6} \frac{VR^3}{\lambda} \rho s_A h \frac{l_x}{l_y} U_\infty^3 \qquad (C19)$$

Acknowledgments

References

[1] Kuchemann, D., *The Aerodynamic Design of Aircraft*, Pergamon, New York, 1978.

[2] Faleiro, L., "Beyond the More Electric Aircraft," *Aerospace America*, Sept. 2005, pp. 35–40.

[3] Crowther, W. J., and Gomes, L. T., "An Evaluation of the Mass and Power Scaling of Synthetic Jet Actuator Flow Control Technology for Civil Transport Aircraft Applications," *Proceedings of the Institution of Mechanical Engineers, Part I (Journal of Systems and Control Engineering)*, Vol. 222, No. 5, 2008, pp. 357–372.
doi:10.1243/09596518JSCE519

[4] Ning, S. A., and Kroo, I., "Multidisciplinary Considerations in the Designs of Wings and Wing Tip Devices," *Journal of Aircraft*, Vol. 47, No. 2, 2010, pp. 534–543.
doi:10.2514/1.41833

[5] Liscouët-Hanke, S., Mare, J.-C., and Pufe, S., "Simulation Framework for Aircraft Power System Architecting," *AIAA Journal*, Vol. 46, No. 4, 2009, pp. 1375–1380.doi:10.2514/1.41304

[6] Liscouët-Hanke, S., Pufe, S., and Mare, J-C., "A Simulation Framework for Aircraft Power Management," *Proceedings of the Institution of Mechanical Engineers, Part G (Journal of Aerospace Engineering)*, Vol. 222, No. 6, 2008, pp. 749–756.
doi:10.1243/09544100JAERO342

[7] Warsop, C., Hucker, M., Press, A. J., and Dawson, P., "Pulsed-Air Jet Actuators for Flow Separation Control," *Flow, Turbulence and Combustion*, Vol. 78, Nos. 3–4, 2007, pp. 255–281.
doi:10.1007/s10494-006-9060-4

[8] Bolzmacher, C., Bauer, K., Schmid, U., Hafez, M., and Seidel, H., "Displacement Amplification of Piezoelectric Microactuators with a Micromachined Leverage Unit," *Sensors and Actuators A (Physical)*, Vol. 157, No. 1, 2010, pp. 61–67.
doi:10.1016/j.sna.2009.10.014

[9] Moreau, E., "Airflow Control by Non-Thermal Plasma Actuators," *Journal of Physics D: Applied Physics*, Vol. 40, Feb. 2007, pp. 605–636.
doi:10.1088/0022-3727/40/3/S01

[10] Crowther, W. J., "Control of Separation on a Trailing Edge Flap Using Air Jet Vortex Generators," *Journal of Aircraft*, Vol. 43, No. 5, 2006, pp. 1589–1592.
doi:10.2514/1.15755

[11] White, F. M., "Viscous Flow in Ducts," *Fluid Mechanics*, 3rd ed., McGraw-Hill, New York, 1979, pp. 356–357.

[12] Crook, A., and Wood, N. J., "Measurements and Visualizations of Synthetic Jets," AIAA Paper 01-0145, Jan. 2001.

[13] Glezer, A., and Amitay, M., "Synthetic Jets," *Annual Review of Fluid Mechanics*, Vol. 34, Jan. 2002, pp. 503–529.
doi:10.1146/annurev.fluid.34.090501.094913

[14] Bridges, A., and Smith, D. R., "Influence of Orifice Orientation on a Synthetic-Jet Boundary-Layer Interaction," *AIAA Journal*, Vol. 41, No. 12, 2003, pp. 2394–2402.
doi:10.2514/2.6838

[15] Amitay, M., and Glezer, A., "Aerodynamic Flow Control Using Synthetic Jet Actuators," *Control of Fluid Flow*, Lecture Notes in Control and Information Sciences, Springer, New York, 2006, pp. 45–74.

[16] Amitay, M., Smith, D. R., Kibens, V., Parekh, D. E., and Glezer, A., "Aerodynamic Flow Control over an Unconventional Airfoil Using Synthetic Jet Actuators," *AIAA Journal*, Vol. 39, No. 3, 2001, pp. 361–370.
doi:10.2514/2.1323

[17] Rusovici, R., and Lesieutre, G. A., "Design of a Single-Crystal Piezoceramic-Driven Synthetic-Jet Actuator," *Smart Structures and Materials*, Proceedings of the SPIE, Vol. 5390, Nov. 2004, pp. 276–283.
doi:10.1117/12.539576

[18] Dearing, S., Lambert, S., and Morrison, J., "Flow Control with Active Dimples," *The Aeronautical Journal*, Vol. 111, No. 1125, 2007, pp. 705–714.

[19] Engert, M., and Nitsche, W., "Active Cancellation of Tollmien–Schlichting Instabilities up to $M = 0.40$," International Congress of the Aeronautical Sciences, Paper 2008-3.10.2, Sept. 2008.

[20] Sturzebecher, D., and Nitsche, W., "Active Cancellation of Tollmien–Schlichting Instabilities on a Wing Using Multi-Channel Sensor Actuator Systems," *International Journal of Heat and Fluid Flow*, Vol. 24, No. 4, 2003, pp. 572–583.
doi:10.1016/S0142-727X(03)00051-1

[21] Saric, W. S., "Control of Transition in Swept-Wing Boundary Layers Using MEMS Devices as Distributed Roughness," U.S. Air Force Office of Scientific Research, TR XAA0034F, Arlington, VA, Aug. 2001.

[22] Bolzmacher, C., Riedl, X., Leuckert, J., Engert, M., Bauer, K., and Nitsche, W., "Mechanically Amplified Piezoelectric Microactuators for Laminar-Turbulent Transition Control on Airfoils," *Journal of Microelectronics and Electronic Packaging*, Vol. 6, No. 4, 2009, pp. 211–218.

[23] Jukes, T., Choi, K-S., Johnson, G. A., and Scott, S. J., "Turbulent Drag Reduction by Surface Plasma Through Spanwise Oscillation," AIAA Paper 06-3693, June 2006.

[24] Bernard, N., Balcon, N., and Moreau, E., "Electric Wind Produced by a Single Dielectric Barrier Discharge Actuator Operating in Atmospheric Flight Conditions—Pressure Outcome," AIAA Paper 08-3792, June 2008.

[25] Bernard, N., Balcon, N., and Moreau, E., "Electric Wind Produced by a Surface Dielectric Barrier Discharge Operating over a Wide Range of Relative Humidity," AIAA Paper 09-0488, Jan. 2009.

[26] Santin, M., Traverso, A., and Massardo, A., "Technological Aspects of Gas Turbine and Fuel Cell Hybrid Systems for Aircraft: A Review," *The Aeronautical Journal*, Vol. 112, No. 1134, 2008, pp. 459–467.

[27] Moir, I., and Seabridge, A., "Electrical Systems," *Aircraft Systems: Mechanical, Electrical and Avionics Subsystems Integration*, 3rd ed., Wiley, New York, 2008, pp. 199–202.

[28] Epstein, A., "Millimeter-Scale, MicroElectroMechanical Systems Gas Turbine Engines," *Journal of Engineering for Gas Turbines and Power*, Vol. 126, Apr. 2004, pp. 205–226.

doi:10.1115/1.1739245

[29] Kang, S., "Fabrication of Functional Mesoscopic Ceramic Parts for Micro Gas Turbine Engines," Ph.D. Thesis, Stanford Univ., Stanford, CA, 2001.

[30] Rudolph, P. K. C., "High-Lift Systems on Commercial Subsonic Airliners," NASA CR-4746, Sept. 1996.

[31] Wedderspoon, J., "The High-Lift Development of the A320 Aircraft," International Congress of the Aeronautical Sciences, Paper 1986-2.3.2, Sept. 1986.

[32] Briére, D., "Overview on Airbus Fly by-Wire Status," *Air and Space Europe*, Vol. 3, Aug. 2001, pp. 178–179.
doi:10.1016/S1290-0958(01)90087-5

[33] Greene, D. L., "Energy-Efficiency Improvement Potential of Commercial Aircraft," *Annual Review of Energy and the Environment*, Vol. 17, Nov. 1992, pp. 537–573.
doi:10.1146/annurev.eg.17.110192.002541

[34] Gardenghi, R. A., Houlne, R. C., Keggins, B. G., Wilson, L. E., and Maerten, K. R., "A High Reliability Compact Lightweight High Voltage Transformer," *Proceedings of the Twenty-First International Power Modulator Symposium*, Institute of Electrical and Electronics Engineers, Piscataway, NJ, 1994, pp. 210–213.

[35] Jackson, P., "Aero-Engines," *Jane's All the World's Aircraft 1998–1999*, 1998, p. 790.

[36] "Type Certificate Data Sheet E29NE," Model CFM56-5, Federal Aviation Administration, U.S. Department of Transportation, Apr. 1998.

[37] "Friction Losses for Fully Developed Flow in Straight Pipes," IHS ESDU, Std. ESDU 66027, London, Sept. 1966, Amendment E, March 2007.

[38] Bent, R. D., and McKinley, J. L., "Installation and Maintenance of Electrical Systems," *Aircraft Electricity and Electronics*, 3rd ed., McGraw–Hill, New York, 1981, pp. 174–177.

[39] McLean, J. D., Crouch, J. D., Stoner, R. C., Sakurai, S., Seidel, G. E., Fiefel, W. M., and Rush, H. M., "Study of the Application of Separation Control by Unsteady Excitation to Civil Transport Aircraft," NASA CR-209338, Sept. 1999.

[40] Hunt, E. H., Reid, D. H., Space, D. R., and Tilton, F. E., "Commercial Airliner Environmental Control System. Engineering Aspects of Cabin Air Quality," *Proceedings of the Sixty-Sixth Aerospace Medical Association Annual Meeting*, May 1995, http://www.boeing.com/commercial/cabinair/ecs.pdf [retrieved 5 Dec. 2009].

[41] Godard, G., and Stanislas, M., "Control of a Decelerating Boundary Layer. Part 3: Optimization of Round Jets Vortex Generators," *Aerospace Science and Technology*, Vol. 10, Sept. 2006, pp. 455–464.
doi:10.1016/j.ast.2005.11.005

[42] Jabbal, M., and Zhong, S., "The Near Wall Effect of Synthetic Jets in a Boundary Layer," *International Journal of Heat and Fluid Flow*, Vol. 29, No. 1, 2008, pp. 119–130.
doi:10.1016/j.ijheatfluidflow.2007.07.011

[43] Schaeffler, N. W., "The Interaction of a Synthetic Jet and a Turbulent Boundary Layer," AIAA Paper 03-0643, Jan. 2003.

[44] Bray, T. P., and Garry, K. P., "Optimization of Air-Jet Vortex Generators with Respect to System Design Parameters," *The Aeronautical Journal*, Vol. 103, No. 1028, 1999, pp. 475–479.

[45] Rathnasingham, R., and Breuer, K. S., "Active Control of Turbulent Boundary Layers," *Journal of Fluid Mechanics*, Vol. 495, Nov. 2003, pp. 209–233.
doi:10.1017/S0022112003006177